Proceedings of ICRC 2001: 2127 © Copernicus Gesellschaft 2001

ICRC 2001

Preliminary results from the first flight of ATIC: The silicon matrix

J. H. Adams Jr. for the atic collaboration and for the atic collaboration

NASA Marshall Space Flight Center, Huntsville, AL 35812, USA

Abstract. The Advanced Thin Ionization Calorimeter (ATIC) uses a silicon matrix detector in conjunction with a scintillator hodoscope to determine the incident cosmic ray's charge. Cosmic rays that interact in a carbon target have their energy determined from the shower that develops within a fully active calorimeter composed of a stack of scintillating BGO crystals. The silicon matrix consists of 4480 individual silicon pads, each capable of measuring the signal from cosmic rays with atomic numbers from 1 to 26. Preliminary results will be presented describing the performance of the silicon matrix during the 16-day maiden flight of ATIC around Antarctica.

1 Introduction

The silicon matrix is designed to provide individual elemental resolution from H to Fe. It is located on top of the Advanced Thin Ionization Calorimeter (ATIC) experiment (Wefel et al., 2001) shown in fig. 1. It must detect all incident particles within the ATIC aperture, including those incident at zenith angles up to 57°. To separate the lightest elements, care must be taken about the additional signal due to radiation scattered back from the calorimeter. For this reason the matrix must be a mosaic of small detector pads so that the pad containing the signal from the incident particle is likely to have little or no additional signal. Simulations of ATIC have predicted that for detector pads as small as 3 cm², the fraction of misidentified protons is less than 2% in the energy range 10 GeV to 100 TeV due to backscatter (Seo et al., 1996 and Ganel et al. 1999).

Corresponcence to: J. H. Adams, Jr.
{james.h.adams@msfc.nasa.gov)

2 Description of the Matrix

The matrix consists of four planes of detectors. The active detector areas in these planes are partially overlapped to completely cover the aperture. The matrix is built from four-pad silicon detectors mounted on daughter boards with 28 daughter boards mounted on a motherboard. The motherboards are multi-layer circuit boards 109 cm long and 6.634 cm wide that also carry the front-end electronics for the detectors. Detector ladders consist of two motherboards with one inverted over the other and offset so the active detector areas partially overlap. Two motherboards belonging to a ladder are shown in fig. 2. The matrix has two panels of ladders with 10 ladders on each. These panels face each other with the ladders mounted offset so that the active areas of the ladders partially overlap. The active area of the matrix is 99.21cm by 107.86 cm.

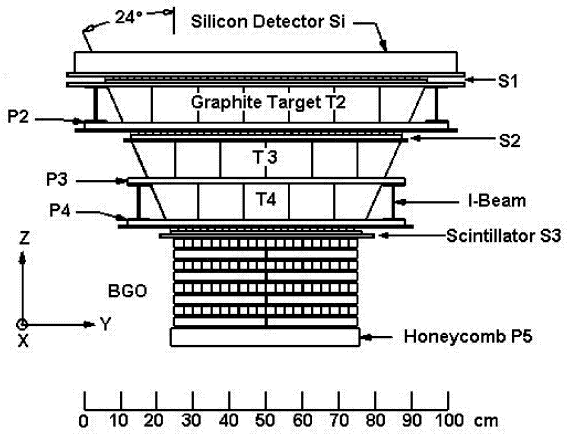

Fig. 1. The ATIC instrument configuration

2.1 Detector Selection

The four-pad detectors are made on 10 cm polished wafers of float-zone silicon (Wacker, 1997). The wafers are 380μm thick with a rms variation of 5μm (which corresponds to 0.17 charge units at Fe). The thickness variation within wafers is <3.5μm. The silicon is phosphorous-doped with a resistivity of >5000Ωcm. Three four-pad detectors were made on each wafer. The active areas of the detector pads are 1.945 cm by 1.475 cm. The detectors are PIN diodes. A common blocking contact is created on one side by phosphorous diffusion while the individual detector pads are created on the other by etching apertures into a silicon dioxide layer. Rectifying contacts are created in these apertures by boron ion implantation. After aluminum contacts are deposited, the whole surface is passivated with silicon dioxide. The finished detectors are tested on wafer with automated probe stations for full depletion and leakage current. After sawing they are tested once more before being mounted on ceramic daughter boards and wire bonded. Selected daughter boards (DBs) must have a leakage current per detector pad of <100 nA at 100 volts. Also the leakage current should not increase at a rate >3% per volt at 120 volts. The nominal capacitance of each detector pad is 90 pF. All the pads on selected DBs must fully deplete at a bias <80 volts.

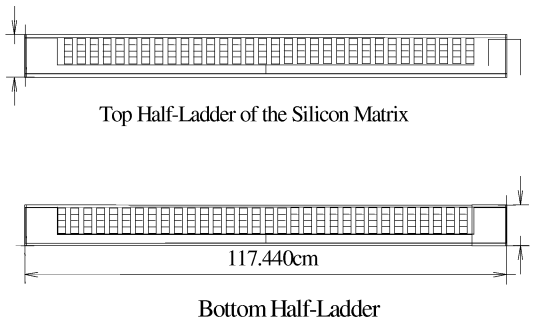

Fig. 2. This figure shows two motherboards that make up a ladder of the silicon matrix. The top half-ladder is inverted and placed over the bottom half-ladder so that the detectors are offset by half a pitch. The detectors are spaced so that they slightly overlap within the ladder. This makes the ladder continuously sensitive over its length.

The noise was measured on DBs that meet the above criteria. Each pad was connected to a preamp, shaper and pulse height analyzer. Charge pulses were injected at the detector and the peak width of the pulses was measured. This measurement was repeated with an equivalent capacitor replacing the detector to correct for electronic noise. This resulted in a distribution of measured noise levels over the ensemble of measurements with the most probable detector noise being 1320 electrons. Detectors with noise <8100 electrons were selected for use in ATIC.

On many DBs the pads were also checked with a beam of relativistic electrons (2.27 > E >1.55 MeV) from an ^{90}Sr source normally incident on the detector. In each case the location of the electron peak was measured. Variations in the electron peak location in the detectors tested were found to be consistent with the variation in wafer thickness.

2.2 Front-end Electronics

There is one front-end channel per detector pad consisting of a charge-sensitive amplifier, a shaping amplifier and track and hold circuit. These reside in 16-channel application-specific integrated circuit (ASIC) chips called CR-1 chips (Adams et al.,1999). The 16 channels are multiplexed to a common output buffer on the chip. Tests of this chip have shown that the rms noise is 4000 electrons. There are 7 CR-1 chips per motherboard. Following a master trigger, these are multiplexed in turn onto a common data line that leads to a grandmother board (GMB) circuit located outside the matrix. The GMB digitizes the signals and places them in an output register. The GMB also periodically calibrates each channel with accurately known charge pulses. Each GMB has 10 circuits to support motherboards. Each GMB is connected to two ASIC Control Logic Boards (ACLBs) that control data from the GMB output registers. Each signal is compared to the pedestal measured for that channel. When the signal exceeds a threshold above the pedestal it is buffered into the data system. The threshold for each channel is set digitally by the ACLB according to the equation $T_i = A + B_i$ where T_i is the threshold on the ith channel, A is a universal threshold and B_i is a correction factor for each channel. B_i can be positive or negative. Pre-flight simulations indicated that this sparsification strategy will reduce the data volume by a factor of ~ 100.

3 Simulated Detector Performance

The performance of the matrix was simulated using GEANT (Brun et al., 1984). The energy deposition in the silicon detectors was calculated in two parts. The energy loss restricted to the creation of electrons below 10 keV was calculated using the Bethe-Bloch formula. The energy going into higher energy electrons was used to create delta rays that were tracked by GEANT as secondary particles.

3.1 Sparsification Efficiency

The threshold for keeping a detector signal must be selected to maximize the retention of signals from events without keeping noise. To check this, we simulated 100 GeV cosmic ray protons arriving isotropically within the aperture of ATIC. We also simulated 4479 noise signals for each event. All the signals included a combined noise of 4700 electrons from the CR-1 chip, the detectors, and

the ADC. The proton signals also include the silicon detector thickness variation. The noise and the proton signals were well separated. We found that by setting a threshold set at channel 14, all the protons were detected and 99% of the noise was rejected. With this threshold setting, event records will contain 45 noise signals, on average, in addition to the proton signal.

3.2 Misidentification

GEANT simulations have shown that the incident particle can be located in the matrix with an rms error of 2 cm above 1 TeV from shower core measurements only. In 2/3 of the cases additional information from the plastic scintillator layers can reduce this to about 1 cm. While the misidentification probabilities have not been estimated for the detector pad size we are using, estimates were made earlier for 3 cm by 3 cm pixels. Combining these estimates with a 2 cm location error, we estimate that the misidentification probability is 1.4% at 10 TeV. With pixels less than half this size and better locations for 2/3 of the events, we expect the misidentification probability to be smaller at 10 TeV and less and 2% even at 100 TeV.

3.3 Elemental Resolution

GEANT was used to simulate the energy deposited by protons. The signal from ions of charge Z was simulated by summing the energy deposited by Z^2 protons. Space does not permit the results to be shown here, but they indicated that we should expect clear separation between all the elements from Z=1 to 26.

4 Preliminary Experimental Results

ATIC was launched from the Ross Ice Shelf in Antarctica on 28 December 2000 and flew around Antarctica, landing just beyond the Trans-Antarctic mountain range on 13 January 2001. The average atmospheric overburden during the flight was 6 g/cm^2. The data set from the flight contains approximately 25 million events.

The operating modes of the silicon matrix include one in which the sparsification function is turned off. Before the flight, we tested ATIC by triggering on cosmic ray muons and collecting data with sparsification turned off. The result was that we read out every pixel in the matrix on every trigger. This allowed us to locate the pedestal. It also allowed us to determine the location of the MIP peak from the muons passing though the silicon pixels. We found that the pedestal distribution was well fit by a Gaussian, as we expected. From this fit we were able to determine the RMS noise on each channel. From our examination of the pedestal distributions and the MIP peak, we were able to determine the optimum value for the A parameter in the threshold equation above. We were able to achieve 99% sparsification efficiency with >99% efficiency for the detection of singly charged particles in these ground tests. Similar test data was acquired during the initial portion of the flight, but we have not examined it yet.

Another of the operating modes of the matrix is to measure the pedestals for all the detectors. This was done once every six minutes during the flight. We also did this during the muon runs and compared the pedestal values measured in this way with those determined from the un-sparsified muon data. The results showed that both measures of the pedestal locations agreed within ±1 channel. The only significant offsets were for the first channels read out. This is a problem with the CR-1 chip design that had been previously discovered. Applying the B_i corrections is a known fix for it. Initial results from the flight data indicate that the pedestals were tracked well by the in-flight measurements.

We have used the data to investigate the interference from backscatter. We have found that, as expected, the amount of backscatter increases with energy deposited in the calorimeter. We examined the backscatter pattern for one large event (shown in fig. 3). This event deposited 87 TeV in the calorimeter so it is among the biggest we expect to observe with ATIC. The figure shows hits with signals >3 MIPs. Three MIPs is approximately the threshold for separating protons and helium.

In preflight simulations we investigated how well we could fit the shower axis and predict the location of the primary signal in the silicon matrix. We found the location precision improved with energy. We estimated that 2-3% of the protons at 100 TeV would be misidentified as protons. We found that typically we could fit a shower well enough to locate the primary signal within a 3X3 group of pixels.

We do not know the predicted location of the primary's signal in the matrix for this 87 TeV event. If we pick a location in the matrix at random and assume we must search a 3X3 array of pixels, we can see that most cases the search area does not contain a backscatter signal that would be mistaken for helium. There are 4212 choices for the location of the center of the 3X3 pattern in the matrix. In only 301 of these locations will the 3X3 pattern contain a pixel with a signal > 3 MIPs. So if we assume the incident cosmic ray is a proton, we can say that a priori, there is a 7% probability that it will be mistaken for helium because of backscatter. This is somewhat higher than we predicted partly because we chose a relatively large search area. Such high energy events can often be fit well enough to reduce the search area to 2X2 pixels.

In the above analysis, we assumed that the backscatter is uncorrelated with the primary signal location. However, our simulations have shown this assumption to be unreliable. Quite often there is a concentration of backscatter in the general area of the primary single. For these reasons, we cannot determine the misidentification probability for this event without further analysis.

We also examined 334 events that deposited more than 1.5 TeV in the calorimeter. We accumulated the number

of hits in each pixel that exceeded 3 MIPs in any pixel in the matrix and found that the probability of any one pixel having a signal > 3 MIPs was 0.00088. If we neglect the signals from helium and heavier primaries and assume that all these signals are due to backscatter, we can estimate the probability that any 3X3 pixel pattern will contain a backscatter signal. This probability is 0.8%. It is tempting to assume this is the probability of misidentifying a proton as a helium for events with deposited energies > 1.5 TeV, but as pointed out above, our pre-flight simulations show a tendency for the backscatter to cluster in the general vicinity of the primary signal. This will increase the probability of misidentification so we should regard 0.8% as only an estimate of the lower bound for misidentification.

5 Conclusions

We have described the first large area silicon matrix developed for cosmic ray research. We have shown the measured detector performance and simulations of the sparsification efficiency, misidentification probability and elemental resolution. The results show that the signals of interest can be separated from noise, and the design has adequate resolution and background rejection to identify the atomic numbers of the incident cosmic rays from protons to iron.

Acknowledgements. This work was supported by NASA grants to LSU, NRL, SU and UMD. We thank NASA WFF, NSBF and the NSF Polar program for the balloon flight.

References

Adams, J. H., Jr. et al., Silicon Matrix Detector for ATIC, Vol. 4, pp. 76, *26th ICRC*, 1999

Brun, R. et al. 1984, *User's Guide, CERN, DD/EE/84-1*, Geneva.

Ganel, O. et al. 1999, *in Space Technology and Applications International Forum*, ed. M. El-Genk, AIP Conference Proceedings, 458, 272-2777.

Seo, E. S. et.al. 1996, *in Gamma-Ray and Cosmic Ray detectors, Techniques, and Missions*, Ed. By B.D. Ramsey and T. A. Parnell, Proc. SPIE Intl. Symp. on Optical Sci., Eng., and Instr., Vol. 2806, pp. 134-144.

Wacker Siltronics 1997, Burghausen, Germany.

Wefel, J. P., The ATIC Experiment: First Flight, *this conference*, 27th ICRC, OG 1.1, 2001

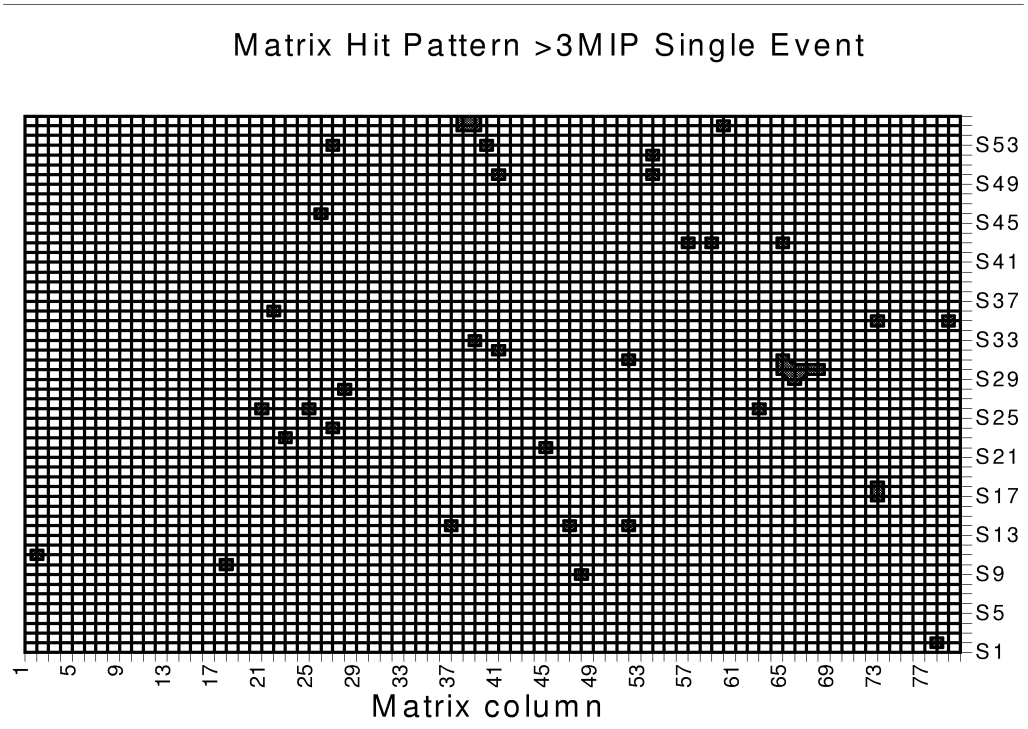

Fig. 3 This figure shows the pattern of hits in the silicon matrix from a single event. Each grid intersection corresponds to a single pixel in the matrix. This event has a deposited energy in the calorimeter of 87 TeV. The hit threshold is 3 MIPs, the typical dividing line between protons and helium.